Experimental and multi-scale investigation of the mechanical behavior of mechanically recycled glass fiber reinforced thermoplastic composites

Saïf Eddine Sekkal[a,b], Fodil Meraghni[a], George Chatzigeorgiou[a], Laurent Peltier[a], Nelly Durand[b]

[a] *Arts et Métiers Institute of Technology, CNRS, Université de Lorraine, LEM3-UMR7239, 4 Rue Augustin Fresnel, Metz, 57078, France*
[b] *Cetim, 21 Rue de Chemnitz, Mulhouse, 68200, France*

Abstract

Fiber reinforced thermoplastic polymer composites have gained a lot of attention over the past two decades, due to their excellent mechanical performance and their lightweight resulting in lower CO_2 emissions for airplanes and vehicles. However, with increased demand for these materials, research regarding environmentally friendly recycling routes has become a central environmental issue. Mechanical recycling by exploiting the melting properties of thermoplastic polymers has proven an excellent way of increasing the value of recycled composites, especially compared to other mainstream techniques. This research aims at investigating the relationship between the microstructure of these materials and their resulting mechanical properties. The studied material is processed by compressing molding chopped woven composites chips, made from a polyamide 6 matrix reinforced with glass fibers. A novel microstructural investigation for these types of materials was conducted using multiple destructive and non-destructive techniques, along with tensile and flexural tests on specimens made from different chips sizes. This investigation revealed a hierarchical fiber structure with a mixture of intact woven chips and randomly oriented unidirectional fiber strands. This microstructure causes complex damage propagation mechanisms and variability in mechanical performance. This hinders development and large-scale commercialization of these materials and favors other less eco-friendly recycling strategies. Therefore, developing accurate predictive models for the mechanical response of these materials is important, thus enabling fast design optimization. A multi-scale predictive model is hence proposed based

on extensive qualitative and quantitative microstructural investigation and is able to capture the anisotropy of the material. This approach is validated on experimental data from a recycled PA6/Glass fiber composite and can be applied for other recycled materials in the same manner.

Keywords: Recycled composite materials, Multiscale modeling, Composite microstructural investigation, Compression molding, Tape reinforced thermoplastics

1. Introduction

During the past two decades, continuous fiber reinforced thermoplastic composites have proven to be a good technological solution within the automotive, aerospace, and renewable energy sectors [1, 2, 3]. These materials provide excellent mechanical properties, low manufacturing costs, good impact properties, and excellent recyclability compared to thermoset counterparts [4, 5, 6, 7, 8, 9, 10, 11, 12]. With the scope of applications and demand for these materials ever-growing, research regarding their closed-loop recycling has become a central environmental issue. Furthermore, recent environmental directives aim to limit the amount of waste that is sent to incineration or landfill. Such sociotechnical pressure is expected to significantly grow, which makes the development of sustainable, viable and economically attractive recycling technologies crucial for the survival of the composite industry.

Composite recycling technologies can be broken down into mechanical, thermal, and chemical recycling. The choice of the technology is inextricably linked to the type of material and the application of the recycled product [11, 10]. Indeed, thermoplastic matrices are easier to handle thanks to their meltability, especially compared to thermoset polymers who have a cross-linked structure and are not meltable upon reheating. The recycled material in this study is a thermoplastic polyamide 6 composite, reinforced with glass fibers. This particular polyamide matrix is highly sensitive to its relative humidity (RH) conditions, which affect the glass transition temperature, the rheology and eventually the material's damage mechanisms [13, 14, 15]. In addition, the damage evolution can modify the overall response of the composite by inducing anisotropy [16]. Nevertheless, thermoplastic composites are great candidates for mechanical recycling, which is typically achieved by shredding or cutting up industrial trimmings, offcuts, or end-of-life parts, fol-

lowed by a process of thermocompression or injection molding [12, 4]. This process of shredding and grinding is considered the least costly way of recycling thermoplastic composites [17]. However, several processing parameters such as mold temperature, extruder speed, etc. affect the mechanical properties of the resulting recycled composite. Colucci et al. [18] investigated the effect of mechanical recycling on the mechanical behavior and microstructure of recycled polymeric composites via injection molding after artificial aging. The results indicate that the recycling process and the aging conditions did not significantly affect the final properties and microstructure of the recycled composites. However, the shear intensive injection molding can cause severe fiber attrition, yielding sub-millimeter short fiber composites, with very low impact strength [19, 20].

An alternative mechanical recycling route for thermoplastic composites is to use a more direct approach without prior material homogenization. This is achieved by chopping the material to be recycled into centimeter-sized composite chips and using compression molding to produce simple or complex parts. This has been done by Tapper et al. [21], who evaluated the effects of a closed-loop recycling methodology on the degradation of discontinuous carbon fiber polyamide 6 composite material and showed significant decrease in tensile stiffness and strength over two recycling loops due to fiber misalignment caused by incomplete fiber separation and fiber breakages from high compaction pressures. Multiple scientific works explored this technique as well using long chopped unidirectional carbon fiber thermoplastic tapes [22, 23, 24, 12]. Another variant of this technology has been used by Kiss et al. [9] by co-moulding shredded material as a core layer between continuous fiber skins. These sandwich-like panels had true upcycling potential to achieve original composite laminate properties in flexural and impact loading.

The literature on the prediction of effective properties of mechanically recycled composite materials is realatively scarce. Indeed, modeling the mechanical properties of these materials requires a deep understanding of the process induced microstructure. The difficulty lies in the quantification of the material and geometrical parameters that affect the performance of the recycled composites, such as fiber orientation, fiber length, void content and matrix degradation. On the other hand, various research works on modeling chopped fiber chip reinforced composites have been published. These types of materials resemble recycled thermoplastic composites in the way they are processed and in their subsequent microstructure. Visweswaraiah et al. [25] reviewed the key features of important analytical and numerical modeling

methods used to forecast the mechanical properties of randomly oriented strand composites and their hybrids, with emphasis on predicting stiffness and strength. Harper et al. [26] developed a geometrical modelling scheme to generate realistic random fiber architectures for discontinuous fiber composites, enabling downstream modelling of mechanical properties. Additionally, Tang et al. [27] investigated fatigue behavior for chopped carbon fiber chip-reinforced composites experimentally and numerically. The writers proposed an analysis procedure that links the microstructure to the fatigue behavior of the bulk material [28].

The aim of this present work is to investigate the performance of mechanically recycled thermoplastic composites with respect to tensile and flexural strength, with a particular focus on the impact of chip size, as well as the observed damage mechanisms. An in-depth investigation of the microstructures of these recycled composites is conducted, and a multi-scale full-field model is developed based on these observations to predict their mechanical properties. It is shown that the mechanical properties of the recycled materials are not significantly affected by chip length. The proposed model is compared to experimental data obtained from tensile tests over two perpendicular directions, and it is demonstrated that the material anisotropy could be accurately captured. The materials and experimental methods used in this study are described in Section 2, while Section 3 presents the experimental results and discusses their implications. Finally, Section 4 describes the full-field modeling of recycled thermoplastic composites, highlighting the potential of this approach to enhance the efficiency of the composite recycling process, as well as to accelerate the design of recycled composite materials with improved mechanical properties.

2. Material preparation, microstructural investigation and testing methods

2.1. Materials and recycling process

Recycling ThermoPlastic Composites (RTPC) take advantage of the melting properties of the polymer matrix. However, the technical implementation of this process is not straightforward and requires considerable development to reach a high level of maturity in terms of use. Cetim is a research and technology organization (RTO) that contributed to the development of thermoplastic recycling technologies using mechanical shredding. The recycled

composites presented and studied in this work are manufactured and supplied by Cetim.

Tepex® Dynalite composite laminates are shredded and thermo-pressed to form recycled composite plates. The used Tepex® Dynalite 102-RG600(x)/PA-GF/47% material is manufactured and supplied by Bond-Laminates GmbH (Am Patbergschen Dorn 11-D-59929 Brilon, Germany).

Tepex® PA-GF 1 mm thick woven laminates are cut into 20 x 20 mm squares and rectangular 160 x 20 mm chips to form two types of recycled materials. For this study, the chips are compression molded into two different materials in the form of 5 mm thick sheets. This is achieved using Cetim's "Thermosaïc®" technology [29]. The chips are then manually distributed evenly in the mold to insure proper consolidation. An example of a chip distribution before compression molding is depicted in figure 1. The finished product is formed in two compression stages: the first one pre-heats and pre-compacts the strands with an applied load that doesn't exceed 50 kN, with a lower temperature than the resin's fusion temperature. The second compression is achieved at a higher temperature and a higher load without exceeding 1300 kN to insure proper matrix fusion without undesired squeeze flow. The formed plate is then cooled and ejected at the end of the production line (figure 1).

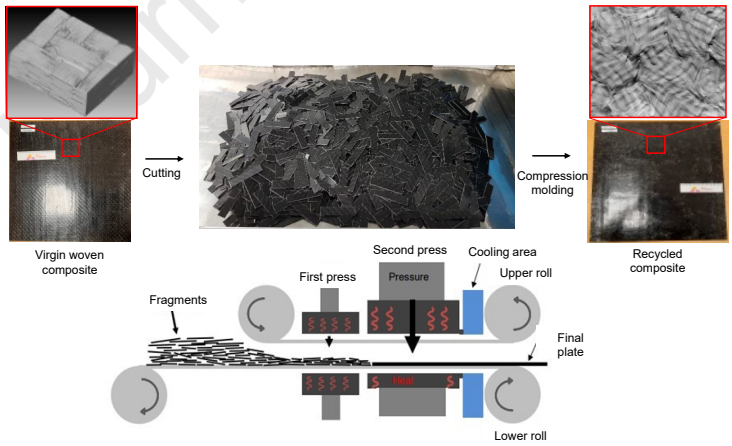

Figure 1: Schematic of the Thermosaïc® production line showing the processing steps for mechanical recycling of thermoplastic composites.

The mechanical performance of these types of materials is inextricably linked to the processing parameters used for their production. These in-

clude the virgin microstructural properties (namely: fiber volume fraction, fiber orientation and aspect ratio), the material shredding process (chip sizes and shapes, material cutting direction), and material thermos-compression parameters (temperature, pressure, step length and dwell time). Choosing the right parameters for optimal mechanical performance presents a challenge and can be costly without the aid of numerical tools for process and mechanical performance modeling.

For the present work, two recycled materials with different chip dimensions are examined. The first one is made out of 20 x 20 mm chips and will be referred to as RTPC-SQR (Recycled ThermoPlastic Composite – SQuaRe chip). The second material is produced from rectangular 160 x 20 mm chips and will be referred to in the rest of this work as RTPC-REC. The aim is to compare these materials with regard to their mechanical properties coupled with an in-depth microstructural investigation to understand the effect of processing. The focus is placed on the RTPC-SQR material with strain field distribution measurements, damage mechanism investigation using X-ray computed tomography (µCT), and modeling of its mechanical performance.

2.2. Microstructural characterization and experimental testing methods

This investigation aims at quantifying the microstructural parameters that affect the performances of recycled composite such as fiber length, fiber orientation, void content, and fiber content [30].

2.2.1. Fiber volume fraction measurements

For two-part composite material systems, one of the most used test methods for determining the fiber volume fraction is the calcination process. The latter is conducted by removing the matrix via ignition, leaving the reinforcement unaffected. For each of the two examined RTPC-SQR and RTPC-REC materials, a pre-weighed 200 x 200 x 5 mm specimen has been cut away from the edge of the composite sheet and placed in a 450°C oven for 24 hours. Specimens before and after the calcination process are portrayed in figure 2a and 2b. By weighing each one of two specimens to the nearest 0.001g and using the manufacturer's specified densities for glass fibers and polyamide 6, fiber volume fractions were calculated using formula 1

$$v_f = \frac{(M_f \times \rho_m)}{(\rho_f - M_f \times (\rho_f - \rho_m))} \tag{1}$$

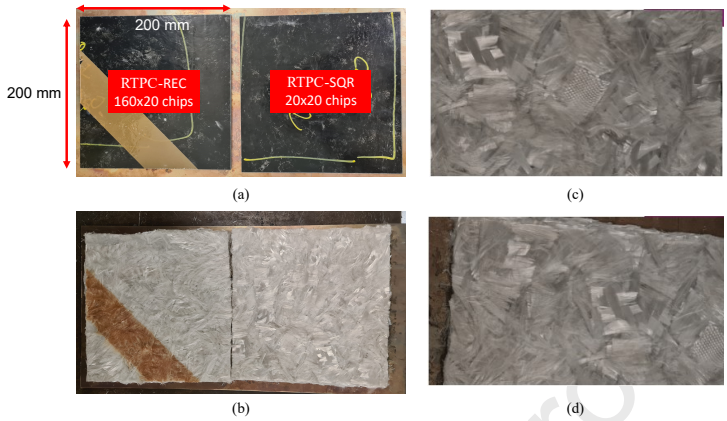

Figure 2: Matrix calcination: (a) and (b) show specimens made with different chip lengths before and after calcination; (c) and (d) show a closeup view of the fiber structure on the surfaces of the specimens.

2.2.2. Optical microscopy investigation

In this optical microscopy investigation, the microstructures of the RTPC-REC and RTPC-SQR are examined in order to compare the materials on a microstructural level and understand the effect of processing and recycling on their microstructures.

To prepare the specimens for observation, three surfaces measuring 22 x 5 mm have been cut from the center of the composite sheets using a Secotum automatic band saw with a blade thickness of 0.5 mm. These specimens are observed through the thickness of the sheet. To prevent overheating that could damage the polymer matrix or generate high loads that could cause fiber breakage, a low cutting speed is chosen during the preparation process. To further protect the thermoplastic matrix from thermal damage, the specimens have been cold mounted using an epoxy Mecaprex KM-U resin. The parameters of the automated polishing machine, including rotation speed and applied pressure, have been carefully chosen to avoid damaging the fibers or the fibers-matrix interface during the polishing and grinding process. This is important due to the differences hardness, between the fibers, matrix, and mounting resin.

Grinding and polishing have been performed in five steps, with water rinsing after each step. The process begins with a 1000-grit silicon carbide, followed by a 4000-grit abrasive. Reducing the particle size from one step to the next helped remove residual subsurface damage. The final three polishing

steps were performed with diamond pads with particle sizes of 9 µm, 3 µm, and 1 µm. By progressively reducing the particle size, the surfaces of the specimens have been carefully polished to a high level of smoothness.

High-resolution micrographs of the specimens have been obtained using a Carl Zeiss Microimaging gmbh 37081 optical light microscope. The motorized stage, with a magnification of 20 and a resolution of 1.35 pixels/µm, is used to take 168 micrographs of each analyzed surface, which are then stitched together to create a complete high-resolution image. It is important to ensure precise sample alignment and constant focus during this large-area microscopy in order to achieve an even resolution over the full specimen. Although the fibers are distinguishable in the stitched images, further image processing has been conducted to improve contrast.

2.2.3. X-ray micro computed tomography investigation of recycled composites

X-ray micro computed tomography (mCT) is a non-destructive technique that has been increasingly used for describing composite materials microstructures [31]. Due to the complex structure of RTPC composites, 3-D observations via X-ray tomography are necessary to get an accurate description of the material microstructure. Multiple analyses have been conducted to first unravel and analyze the microstructures of both RTPC-SQR and RTPC-REC materials, with an emphasis on RTPC-SQR. This non-destructive technique allows for a detailed 3-D observation of these materials, providing valuable insights into the material's microstructure.

To compare the microstructures of RTPC-SQR and RTPC-REC materials, a volume of 125 x 55 x 5 mm has been initially analyzed using X-ray micro computed tomography (mCT). The specimens have been carefully cut from the same area of their respective sheets using a Secotum automatic band saw to ensure consistency in the samples. A spatial resolution of 35.49 µm/pixel is chosen for these initial acquisitions, as it provided a balance between measurement precision and the size of the observed area.

For the porosity measurements and comparison, a higher resolution is required to obtain more accurate results. For this scope, a resolution of 9.46 µm/pixel, corresponding to a volume of 18.5 x 13.5 x 5 mm is chosen. This allows for a detection of finer details of the material's microstructure and quantification of the porosity in a more precise way.

Additionally, X-ray tomography has been used to study the propagation of damage in RTPC-SQR by comparing micrographs before and after testing. This helps to identify weak points in the material that could be targeted for

improvement.

2.2.4. Tensile tests on Recycled ThermoPlastic Composites -SQuaRe (RTPC-SQR) specimens

Monotonic tensile tests have been carried out on the RTPC-SQR composite. Due to the specific microstructure, ensuring that tensile test specimens are representative of the mechanical macroscopic behavior of the material is essential. To achieve this, dog bone specimens with a width of 25 mm and 40 mm are cut from a plate using a water jet cutting machine. The specimens are cut from the center of the plate, in two different directions: the manufacturing direction which will be referred to as 0°, and the perpendicular direction 90°.

The tests have been performed on the universal testing Zwick Roell "Z100" machine. The specimens' shapes are chosen to minimize the stress concentration. The dimensions along with how the specimens are cut are portrayed in figure 3. An extensometer is used to measure displacement. Digital image correlation (DIC) is used to visualize the local displacement fields. Hence, a black and white random speckle pattern is applied on the sample surfaces. The kinematic images are recorded using a charge-couple device (CCD) camera, with an acquisition rate of 30 images per second. A lighting source enhances the contrast in the obtained images. The latter are post processed using the VIC2D image correlation software [32, 33].

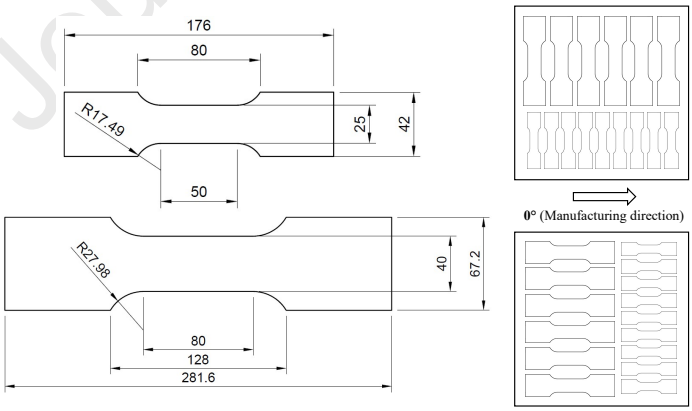

Figure 3: The dimensions of tensile test specimens and the different cutting configurations.

Tests have been carried out at a constant strain rate of 0.01 s^{-1}. Young's modulus is calculated by linear regression between $\varepsilon = 0.05\%$ and $\varepsilon = 0.25\%$

following the BS EN ISO 527-1 standard's recommendation.

2.2.5. Three-point flexural tests on Recycled ThermoPlastic Composites made from square and rectangular chips

Three-point flexural tests have been performed on both RTPC-SQR and RTPC-REC materials. Unlike tensile tests, three-point flexural tests could be performed on wider specimens, which enables testing of a more representative volume, especially for RTPC-REC specimens that are made from 160 x 20 mm chips.

3. Analysis of experimental results

3.1. Fiber volume fraction measurements results

The results of the matrix burn-off tests show that the initial fiber volume fraction of 47% was indeed conserved during processing. This suggests that the processing methods used did not significantly affect the subsequent fiber volume fraction. On the surfaces of both the RTPC-REC and RTPC-SQR samples (figure 2), the woven fiber architecture disappears and randomly oriented meshes are observed. This change in fiber orientation can likely be attributed to the high temperature and pressure levels of the thermocompression process. However, it is worth noting that the woven architecture is partially retained in some areas of the surface, suggesting that it does not completely vanish during processing. These findings provide valuable insights into the effects of thermocompression on the fiber structure for mechanically recycled composites.

3.2. 2-D microstructural investigation results

3.2.1. Qualitative analysis of cross section micrographs of recycled composites

Optical microscopy observations of specimens produced from 20x20 mm and 160x20 mm flakes reveals a microstructure that can be analyzed on two different scales: a microscopic scale and a mesoscopic scale. The main reason for this scale separation is the irregular distribution of the matrix in the material, as shown in figure 4. This heterogeneity is characterized by the presence of regions that are rich in matrix and others that are rich in fibers. At the mesoscopic scale, the fibers form a wave pattern with mostly in-plane orientation. It is possible to distinguish two different strands based on changes in orientation or the presence of matrix-rich regions as shown in

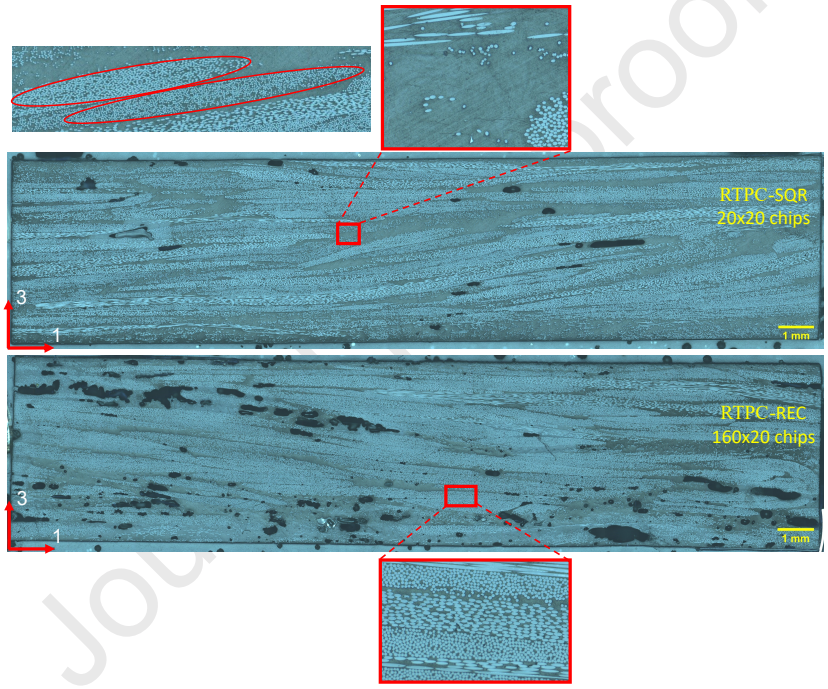

Figure 4: RTPC microstructure captured by optical light microscopy for materials recycled with different chip lengths, and the different observed heterogeneities leading to an analysis by scale separation.

figure 4. At the microscopic level, the structure within the strands is more homogeneous, with multiple fibers having a uniform orientation.

The results of the optical microscopy investigation demonstrate that both RTPC-REC and RTPC-SQR materials present the same microstructural features. However, it is observed that RTPC-REC specimens have more porosity compared to RTPC-SQR. This difference can be traced back to the processing stage. Indeed, during thermocompression, the polymer matrix and the fibers are compressed together. The larger surface area and aspect ratio of the rectangular chips would make them more prone to bending under the applied loads. Therefore, the long rectangular chips could have difficulty to be compressed and aligned properly, leading to less efficient material flow, and more voids and pores in the final composite material.

3.2.2. Quantification of microstructural parameters at the microscale using image processing

The microstructural observations have led to quantitative measurements that aid in numerical simulations later on. This is because the quantitative measurements provide detailed information about the microstructure of the material, including the size, shape, and distribution of the fibers and matrix, which can then be used as input for numerical simulations. This information is crucial for accurately modeling the behavior of the material under different loading conditions and predicting its long-term performance.

In order to accurately determine the fiber volume fraction, measurements have been conducted at both the microscale and mesoscale. At the microscale, 15 random samples of fibers and matrix within strands have been analyzed through image processing illustrated in figure 5a using thresholding techniques shown in figure 5b. This information is used to deduce the strand volume fraction at the mesoscale level through the following formula 2.

$$v_{f/c} = v_{f/s} \times v_{s/c} \tag{2}$$

where $v_{f/c}$ is the fiber volume fraction inside the composite, $v_{f/s}$ is the fiber volume fraction inside the strands, and $v_{s/c}$ is the strand volume fraction inside the composite.

The results are presented in table 1. The strand volume fraction inside the composite is computed assuming the fiber volume fraction inside the composite of 47% obtained by matrix burn-off. This two-level analysis allows for a comprehensive understanding of the microstructure of the composite mate-

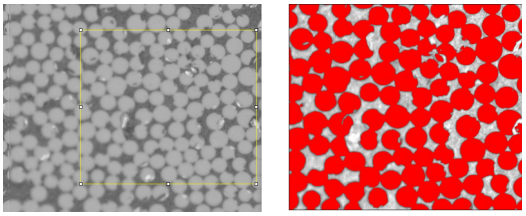

Figure 5: Quantification at the micro level of fiber volume fraction inside the strand using (a) image processing and (b) thresholding techniques.

rial, which is crucial for predicting its mechanical properties using numerical simulation.

$v_{s/c}$ (Std Deviation)	$v_{f/s}$
75.36% (2.70%)	62.36%

Table 1: Results of quantification of microstructural parameters at the microscale using image processing.

3.3. X-ray micro computed tomography investigation results

Through thickness X-ray tomography examination of both materials shows that overall, the woven structure is conserved at the center of the plate in the thickness direction as shown in figure 6. For the RTPC-SQR specimen in figure 6b, the chips can be clearly distinguished. It is worth mentioning that in multiple cases, the woven structure has been deformed from the initial 0° and 90° yarn orientations. This is likely due to material flow effects during thermocompression. For the RTPC-REC specimen in figure 6a, the 160 x 20 mm chips can be distinguished from one another. In some extreme cases, chips seem to have been bent. This is also likely caused by complex mold flow phenomena. Moreover, this has been observed on chips extracted after matrix burn-off (figure 7). Furthermore, on the upper and lower surfaces of the specimens, the woven structure is less present, instead, multiple unidirectional fiber bundles are observed. This is highlighted in figure 8 for a TPRC-SQR specimen, with a comparison between the center and the upper surface of the plate.

Void ratios are also measured and compared for both materials. Tomography observations on RTPC-REC, as depicted in Figure 9a, confirm the

presence of a higher amount of void compared to the RTPC-SQR specimen (Figure 9b).

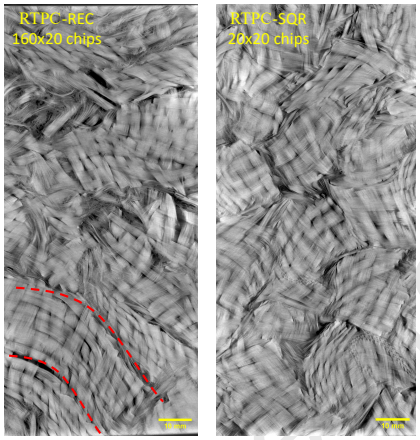

Figure 6: In-plane microstructure comparison of materials recycled from different chip lengths: (a) 160x20 mm and (b) 20x20 mm. The RTPC-REC specimen (a) exhibits multiple bent chips while the RTPC-SQR specimen (b) maintains the initial chip structure.

3.4. Tensile test results for RTPC-SQR specimens

The results for tensile tests are presented as strain-stress curves for different orientations (0° and 90°) presented in figures 10a and 10b, for different specimen widths as shown in figures 10c and 10d and in table 2.

In terms of specimen width effect, for the 90° orientation, the results are similar for 25 mm and 40 mm widths. However, for the 0° orientation, three 40 mm specimens display stiffer mechanical responses compared to other cases.

Regarding the effect of specimen orientation, significant discrepancy in mechanical response is observed between the 0° (manufacturing direction) and the 90° orientations. In fact, specimens that are cut in the 0° orientation display a more rigid behavior compared to the 90° specimens, as has been observed in both 25 mm and 40 mm wide specimens. This can be attributed to the complex material flow inside the mold during thermocompression, that has likely oriented more fibers closer to the 0° direction, making it stiffer.

The above leads to the conclusion that the RTPC-SQR material is not macroscopically transversely isotropic as was expected, but rather anisotropic,

Figure 7: Examples of bent chips retrieved from specimens after matrix burn-off processed from 160x20 mm chips.

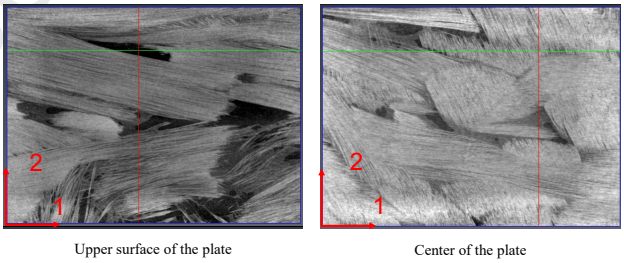

Figure 8: Comparison of the fiber structures on the upper surface and the center of the plate for an RTPC-SQR specimen using micrographs obtained by X-ray micro-computed tomography.

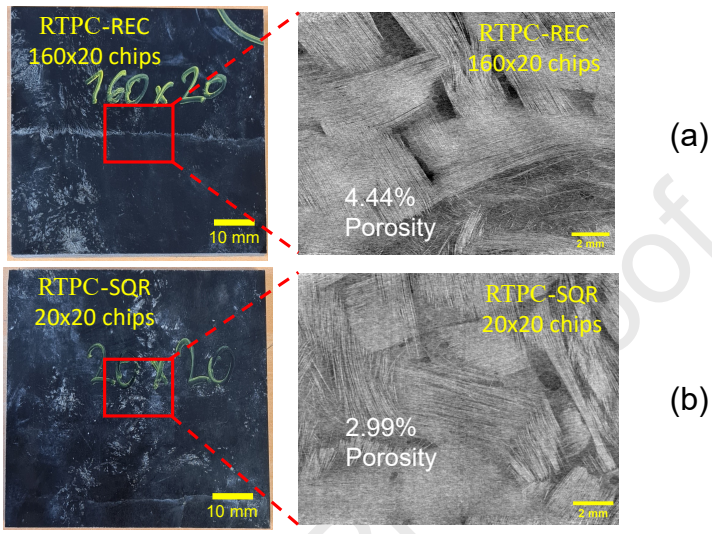

Figure 9: X-ray micro-computed tomography investigation enabling a qualitative and quantitative comparison of recycled materials using two chip lengths: 160X20 (a) and 20X20 (b).

	Young's modulus mean values in GPa (Standard deviation in GPa)		Maximum stress mean values in MPa (Standard devation in MPa)	
Specimen width	90° Orientation	0° Orientation	90° Orientation	0° Orientation
40 mm	9.03 (1.14)	14.9 (1.84)	58.21 (10.37)	157.34 (28.67)
25 mm	8.47 (0.98)	12.38 (1.14)	68.05 (11.75)	115.15 (24.67)
Average values for both specimen widths	8.69 (1.05)	13.46 (1.91)	63.13 (11.06)	136.24 (26.67)

Table 2: Young's moduli and maximum stress values obtained from the tested RTPC-SQR specimens, along with a comparative analysis of these values for various specimen orientations.

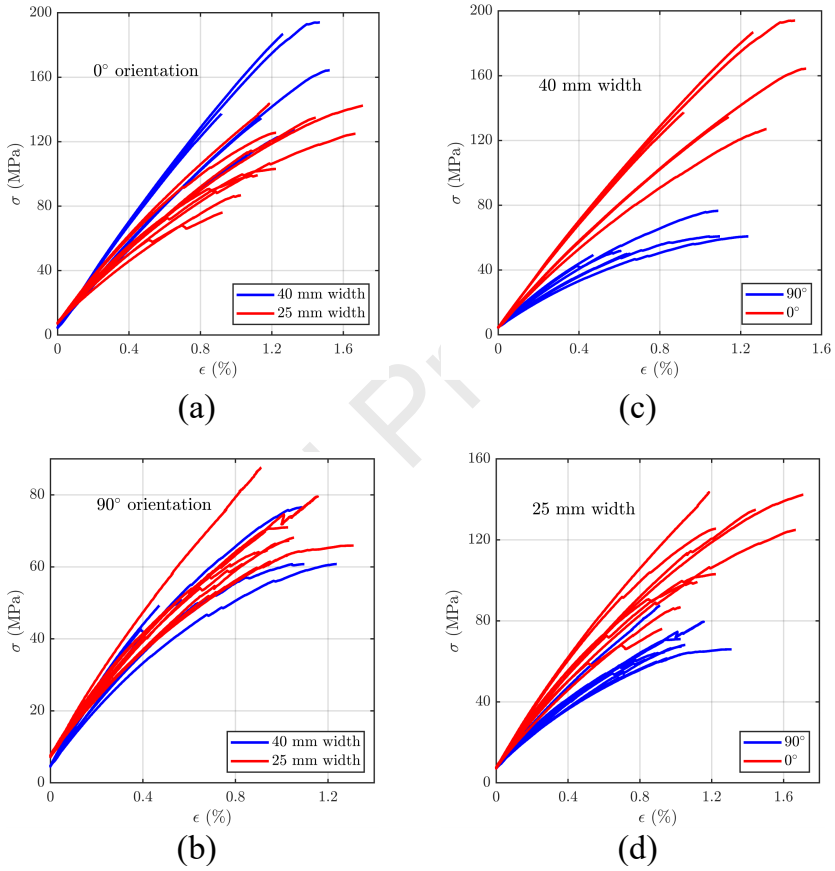

Figure 10: Strain-stress curves performed on the RTPC-SQR material; (a) and (b) show a comparison of mechanical response between specimens with different widths; (c) and (d) highlight a comparison in effective response for different specimen cutting orientations.

and this should be taken into account for the mechanical modeling of this material.

3.4.1. Deformation and damage mechanisms investigation on RTPC-SQR tensile test specimens

X-ray tomography analyses have been conducted on a 40 mm wide dog bone specimen cut at a 90° orientation, before and after the test. The objective is to get a better understanding of where the specimen fails under tension loading. Furthermore, Digital Image Correlation (DIC) captures strain fields and crack propagation in real time. Examination of the specimen pre-loading via X-ray tomography in figure 11 shows that chip woven fiber structure is present alongside multiple fiber bundles. Indeed, the interface between intact chips and randomly oriented fiber bundles can be considered as an area where damage and cracks propagate [12]. This is the case for the examined specimen as shown in figure 11 on observations post failure. Strain fields measurements illustrate how the crack follows a path on the interface between intact woven chips and randomly oriented fiber bundles.

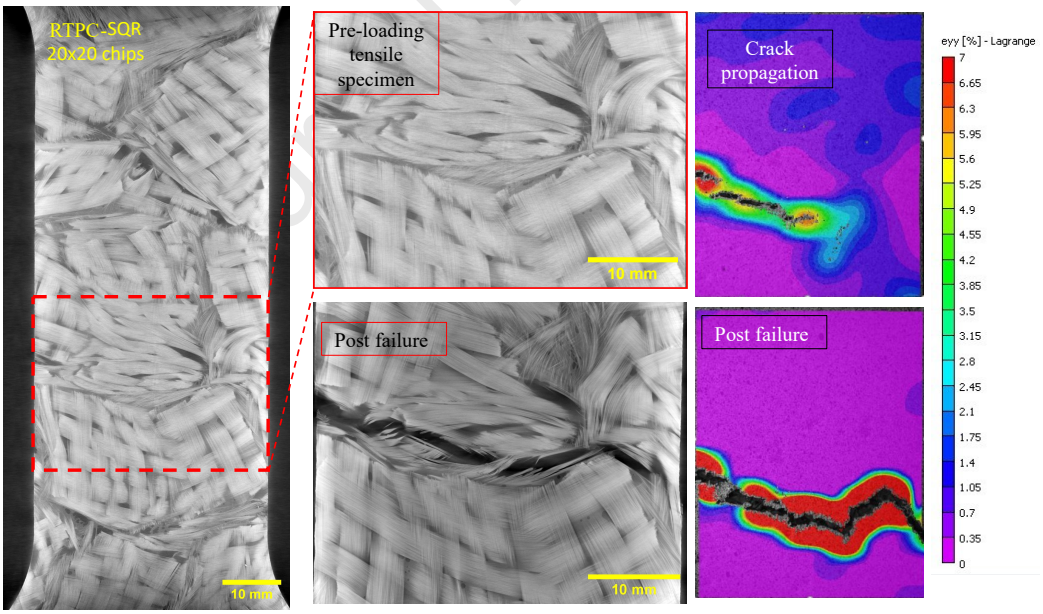

Figure 11: An investigation of damage propagation paths for a TPRC-SQR tensile test specimen using µCT pre-loading and post failure observations coupled with DIC analysis.

3.5. *Three-point flexural test results on Recycled ThermoPlastic Composites made from square and rectangular chips*

The flexural test results of RTPC-SQR and RTPC-REC materials are depicted in Figure 12 as load-displacement curves, providing a visual representation of their mechanical behavior. Both materials exhibit similar responses, suggesting comparable structural integrity and load-bearing capabilities. Supporting this observation, the flexural moduli values in Table 3 quantify the materials' stiffness and resistance to bending forces. Notably, the flexural moduli values for both RTPC-SQR and RTPC-REC materials are consistent, indicating similar mechanical performance.

These experimental findings align with previous studies in the literature [34], which have investigated the influence of the chip size on the mechanical behavior of similar composites. The obtained results confirm that the chip size has limited impact on overall mechanical performance. It is important to note that the chip size of 160x20 mm is not optimal for the recycling process and presents more challenges compared to the use of a chip size of 20x20 mm which resulted in sheets with improved surface conditions.

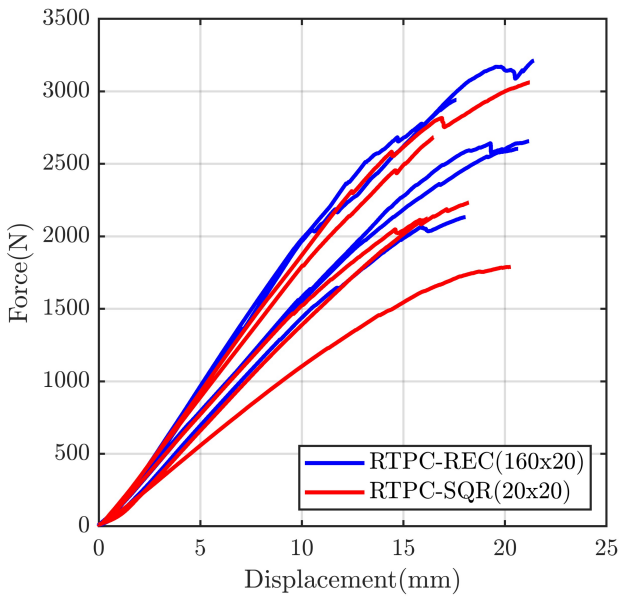

Figure 12: Load-displacement curves for three-point flexural tests performed on specimens recycled using different sized chips.

	Flexural Modulous (GPa)	
	Mean Value	Std Deviation
RTPC-REC (160 x 20 mm chips)	7.90	1.09
RTPC-SQR (20 x 20 mm chips)	7.61	2.10

Table 3: Flexural moduli obtained from three-point flexural tests performed on specimens recycled using different sized chips.

4. Multi-scale full field modeling of Recycled ThermoPlastic Composites

The proposed multi-scale model offers an accurate prediction of RTPC material properties. This model is based on extensive qualitative and quantitative microstructural investigation and is able to captures the anisotropy of the material. The approach is validated through comparisons with experimental results from a recycled Glass fiber – PA6 composite and can be applied for other composites recycled in the same manner.

4.1. Recycled ThermoPlastic Composite Representative Volume Element (RVE) generation tool

Definitions of Representative Volume Elements vary in the literature. In the context of this work, an RVE is considered to be a volume that accommodates a sufficient number of strands, rendering it therefore representative in terms of fiber volume fraction, and fiber orientation. Based on microstructural observations of TPRC materials at different relevant scales, an RVE consisting of multiple randomly oriented strands is chosen to model these media. This modeling strategy is able to capture the behavior of similarly processed materials [28, 27, 35, 36]. The size of the strands is based on the size of the chips used for processing. On the other hand, the volume fraction of strands inside an RVE ($v_{s/c}$) is a microstructural parameter that has been determined through the procedure discussed in section 3.2.2 using image processing. Furthermore, as seen on µCT and optical microscopy micrographs, the strands after thermocompression display a mainly in-plane orientation. Therefore, the strand out-of-plane orientation has been omitted for the RVE generation. This offers the added benefit of generating RVEs with higher strand volume fractions with no intersections between them. Presence of the latter can cause issues in the numerical computations.

The main challenge of TPRC RVE generation for this research is the high value of strand volume fraction that is required ($v_{s/c}$=62%) for an accurate

representation of the real microstructures of these materials. In order to increase the chances of reaching this value, the RVE is constructed in multiple layers, as opposed to placing inclusions in the 3-D RVE.

4.1.1. RVE Generation algorithm: random sequential adsorption

The generation algorithm follows a random sequential adsorption scheme [37]. For each layer, strands are placed sequentially in the RVE, initially with a random orientation using a uniform distribution function, until the required strand ratio is reached. The code has been implemented in MATLAB and exploited the `polyshape` and `intersect` functions to measure whether there are intersections between generated strands.

A Python code is utilized to generate a finite element model, which is based on the information obtained from the Matlab generation code. The latter provides the following information during the generation process: the coordinates of the strand vertices, the orientations of the strands, and the volume fraction of the strands.

Subsequently, the Python code utilizes this data to generate an ABAQUS finite element model that will be meshed later. This involves placing the strands using the vertex information, eliminating the edges of the unit cell, incorporating the matrix material, and assigning material orientations to each individual strand.

Initially, intersections between strands are allowed in order to mimic the exact microstructure of RTPC materials as depicted in figure 6. This is achieved by splitting the generation step into two steps: firstly, strands are placed in the RVE by respecting the periodicity conditions in the boundaries and with no intersections between strands; secondly, more strands are deposited in the center of the RVE, by cutting the areas that intersected with other strands. These generation steps are illustrated in figures 13a and 13c. However, this scheme creates complex shapes (figure 13b) that posed numerous meshing issues using ABAQUS, as shown in figure 13d. In addition to the aforementioned difficulties, there is also the challenge of identifying the material properties that are used in the computations for each of the strands involved when cutting the strands.

The generation process starts by selecting strand center coordinates within the designated generation domain in a random manner. To ensure the periodicity of the RVE, in the case of an intersection with a boundary, the strand is duplicated on the opposite side. For each strand positioned in one of the corners, it is duplicated on all other ones. Additionally, a strand orienta-

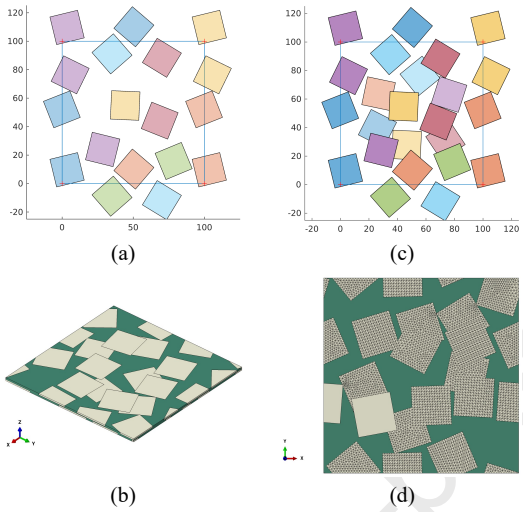

Figure 13: Microstructure generation steps for strands with intersections: (a) generation until saturation with no intersections (b) strands are placed and the intersection area is removed ; (c) and (d) show the errors encountered upon meshing for unit cells with intersecting strands.

tion is chosen based on a specified Orientation Distribution Function (ODF), which is illustrated in figure 18a. For instance, the orientation of the first positioned strand is determined within the range of [-80°, -60°]. Following this, intersections between strands are examined, and if a strand intersects with another, the iteration is terminated, and a counter is incremented to keep track of the number of attempts made. If the maximum number of attempts is exceeded, the current Representative Volume Element (RVE) is discarded, and a new one is generated. This process continues in a loop until the desired volume fraction of strands is achieved. The entire generation process is detailed in the flowchart depicted in figure 14.

4.1.2. Full-field periodic homogenization - theoretical concepts overview

For the considered full-field multiscale approach, the relationship between the microscopic and macroscopic scales is established by averaging the microscopic scale stress and strain over the full domain $\mathcal{B}$:

$$\bar{\sigma} = \frac{1}{V} \int_{\mathcal{B}} \sigma(x) \; dV \tag{3}$$

$$\bar{\varepsilon} = \frac{1}{V} \int_{\mathcal{B}} \varepsilon(x) \; dV \tag{4}$$

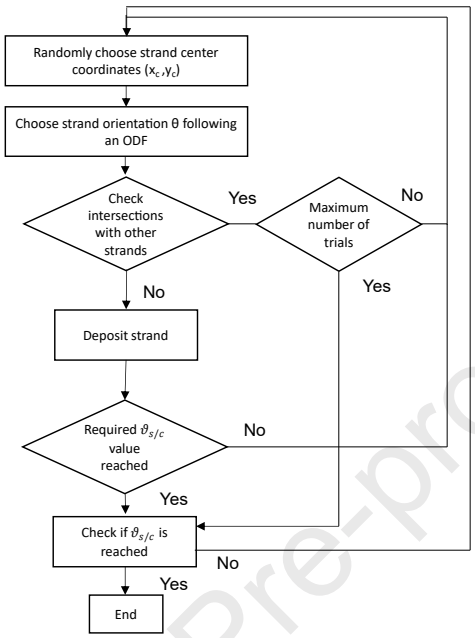

Figure 14: Flowchart detailing microstructure generation process.

where V represents the volume of the unit cell domain $\mathcal{B}$.

Furthermore, the assumption of periodicity inside the unit cell yields the following additive form for the displacement u.

$$\begin{aligned} u\left(x\right) &= \bar{\varepsilon}.x + u'\left(x\right) \\ t_i &= \sigma_{ij} n_j \text{ antiperiodic} \end{aligned} \tag{5}$$

where $\bar{\varepsilon}.x$ refers to the affine part of the displacement; the second term, u' depicts a periodic fluctuation, and $t_i = \sigma_{ij} n_j$ is the traction vector field. Knowing that u' is a periodic function it has the same value at two opposite points x_+ and x_- of the unit cell boundary $\partial\mathcal{B}$.

$$u'\left(x_+\right) = u'\left(x_-\right) \tag{6}$$

Consequently, the part of the strain produced by u' disappears once averaged, rendering the strain average equal to the macroscopic strain.

By substituting 5 into 6, the periodicity boundary conditions (PBCs) for the unit cell can be expressed as a function of the macroscopic strain tensor $\bar{\varepsilon}$ and the displacement u:

$$u'\left(x_+\right) - u'\left(x_-\right) = \bar{\varepsilon}\ .\ \left(x_+ - x_-\right) \tag{7}$$

For more details regarding the theoretical aspects of periodic homogenization, readers are referred to [38, 39, 40, 41, 42, 43, 44]

4.1.3. Numerical periodic homogenization and finite element modeling of TPRC RVEs

For the finite element implementation, PBCs are applied to a meshed RVE by introducing the macroscopic strain $\bar{\varepsilon}$ components. Hooke's law defines the homogenized stiffness matrix in the RVE as $\bar{\sigma}_{ij} = \bar{C}_{ijkl}\bar{\varepsilon}_{kl}$, with $\bar{\sigma}_{ij}$ and $\bar{\varepsilon}_{kl}$ the macroscopic stress and strain tensors respectively. For the identification of the six independent stiffness matrix parameters, six loading cases are implemented using six constraint drivers. A strain value of 1 is applied for each loading case, while the other components of the strain vector are kept at 0, as per eq 8.

$$\begin{bmatrix} \bar{\varepsilon}_{11} \\ \bar{\varepsilon}_{22} \\ \bar{\varepsilon}_{33} \\ 2\bar{\varepsilon}_{12} \\ 2\bar{\varepsilon}_{13} \\ 2\bar{\varepsilon}_{23} \end{bmatrix} = \begin{bmatrix} 1 \\ 0 \\ 0 \\ 0 \\ 0 \\ 0 \end{bmatrix} \rightarrow \begin{bmatrix} \bar{\sigma}_{11} \\ \bar{\sigma}_{22} \\ \bar{\sigma}_{33} \\ \bar{\sigma}_{12} \\ \bar{\sigma}_{13} \\ \bar{\sigma}_{23} \end{bmatrix} = \begin{bmatrix} C_{11} \\ C_{21} \\ C_{31} \\ 0 \\ 0 \\ 0 \end{bmatrix} \tag{8}$$

Finally, the macroscopic stiffness tensor $\bar{C}$ is obtained by computing the macroscopic stress for each one of the six strain states. The deflection modes obtained for each of these elementary strain states are depicted in figure 15.

For this work, an RVE unit cell is composed of four layers. For each layer, the position and orientation of each strand is saved in a text file. The finite element model is created in Abaqus using a python code. The latter creates and assembles the strands for the entire RVE, creates the matrix material and assigns the material properties. The excess strand material over the RVE boundaries is trimmed, and the matrix is assembled with the strands. Afterwards, the material orientation is assigned for each of the strands, and the unit cell is meshed. Linear tetraheadral elements with reduced integration (C3D4) are used for the finite element analysis. Finally, periodic boundary conditions (detailed in section 4.1.2) are applied, and an ".inp" file is generated.

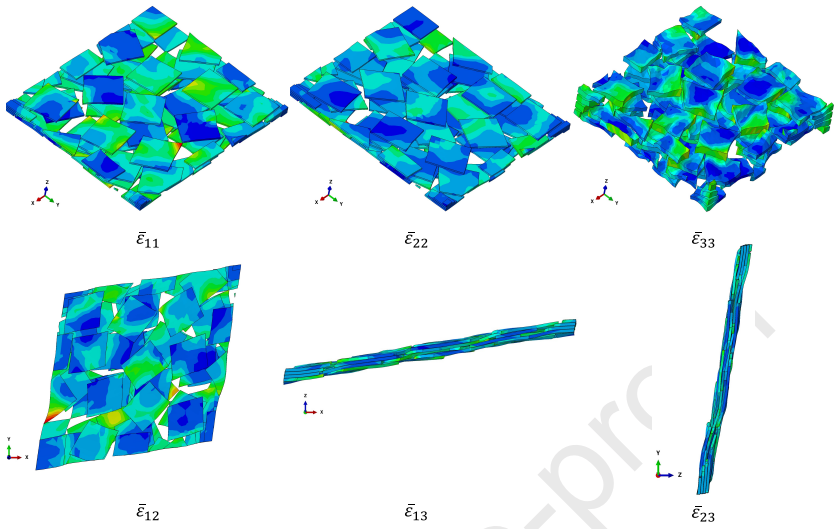

Figure 15: Deflection modes of the unit cell for each of the elementary macroscopic strain states.

Glass fiber	Polyamide 6
$E_f = 81\,000\,\text{MPa}$	$E_m = 3000\,\text{MPa}$
$\nu_f = 0.25$	$\nu_m = 0.3$

Table 4: Glass fiber and Polyamide 6 properties used for the micro-homogenization

4.2. Numerical simulation results

4.2.1. Microscale homogenization and strand material properties

As established via careful microstructural investigation, RTPC materials can be analyzed on two different scales: microscale and mesoscale. At the microscale, the structure consists of a high density of fibers packed tightly. At the mesoscale, multiple strands appear to be imbedded in a matrix solution. Hence the need for modeling at multiple relevant scales. At the mesoscale, the full-field homogenization approach presented in section 4.1.2 is adopted. For microscale modeling, strands were assumed to have a unidirectional structure. This is a result of multiple microstructural observations that illustrate the complexity of the material structure after processing, with some chips retaining a woven structure and others manifesting a unidirectional structure. Glass fiber and PA6 effective properties used for the micro-homogenization are portrayed in table 4.

Furthermore, for the micro-scale homogenization, a mean-field Mori-Tanaka

homogenization scheme is employed to compute the strand material properties [45, 46, 47]. The subsequent recovered elastic constants are utilized for the mesoscale full field homogenization. The full homogenization scheme is portrayed in figure 16.

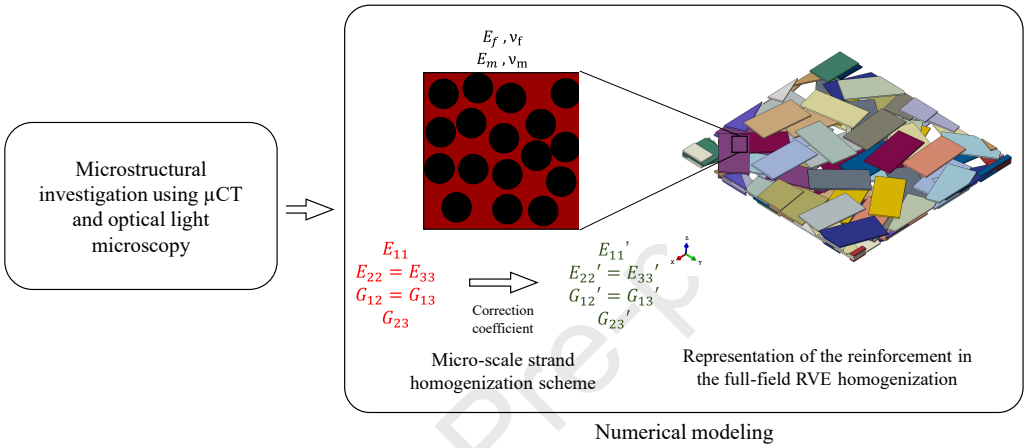

Figure 16: The adopted modeling strategy for mechanically recycled thermoplastic composites using the microstructural investigation.

4.2.2. Results and experimental validation

In order to properly compare the modeling predictions with the tensile test experimental data, three RVEs have been generated using a random strand deposition scheme. A strand volume fraction of 59% is achieved for the three, which gives a value of 79% for the micro-homogenization, that is close to the experimentally measured values.

For these first computations, the anisotropy displayed on RTPC-SQR material, was not predicted in the simulations using randomly oriented strands. Indeed, the values for Young's moduli for the 1 and 2 directions are close to one another as shown in figure 17, which wasn't the case for the tensile tests. This is a consequence of the random orientation that was attributed to the strands during the generation process.

Moreover, multiple previous works showed that mechanical properties of composite materials are inextricably linked to the orientation distribution function (ODF) [48, 49]. Consequently, in order to capture the anisotropy of the RTPC-SQR, a specific ODF has to be imposed on the microstructure generation. This ODF is chosen on the basis of experimental tensile test results

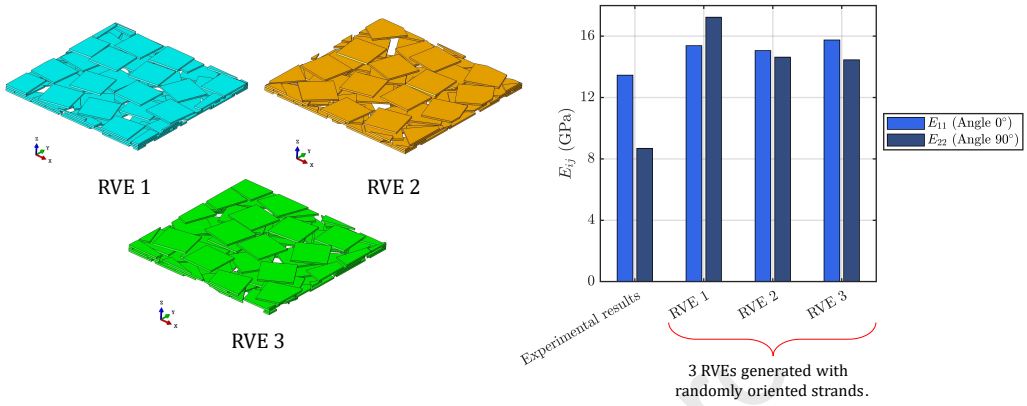

Figure 17: A comparison of experimental and numerical simulation results for three RVEs generated with random strand orientation. The images of RVEs 1,2 and 3 represent the architecture of the reinforcement.

that suggest that more strands should be oriented in 0° direction compared to 90°. A process of fine tuning the model yields a strand generation ODF, plotted in figure 18a, that reproduces the anisotropy of the material as shown in figure 18b.

However, the implementation of the model with the described procedure and the material properties of table 4 leads to overestimation of the mechanical response of RTPC material when compared to experimental data. This could be attributed to the assumption that fibers are perfectly unidirectional inside the strand. This is not the case since fibers sustain noticeable damage during processing that naturally would change their orientations and reduce their properties. This is illustrated in figures 19a, 19b and 19c, which demonstrates the variability of the microstructure at different relative out-of-plane coordinates z* with respect to the total thickness. Additionally, the fiber architecture exhibits a combination of intact woven fibers along with several fiber bundles that deviate from a straight configuration, exhibiting a wavy pattern. An extreme microstructure configuration where different architectures of the reinforcement are present in the recycled composite material is illustrated in figure 19d. This intricate nature of the fiber architectures poses challenges in the modeling. To address this issue, the assumption of strands having a unidirectional (UD) orientation is maintained, and the potential overestimation of the mechanical response is mitigated through a calibration process based on experimental results.

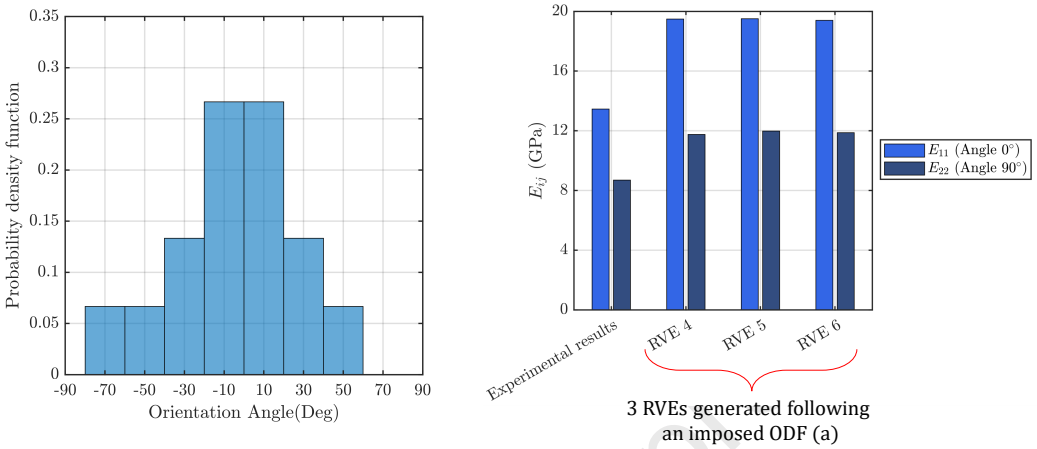

Figure 18: The adopted orientation distribution (ODF) of the reinforcement (a) and Comparison of experimental and the corresponding numerical results (b) for three generated Representative Volume Elements (RVEs), without taking into account correction coefficient.

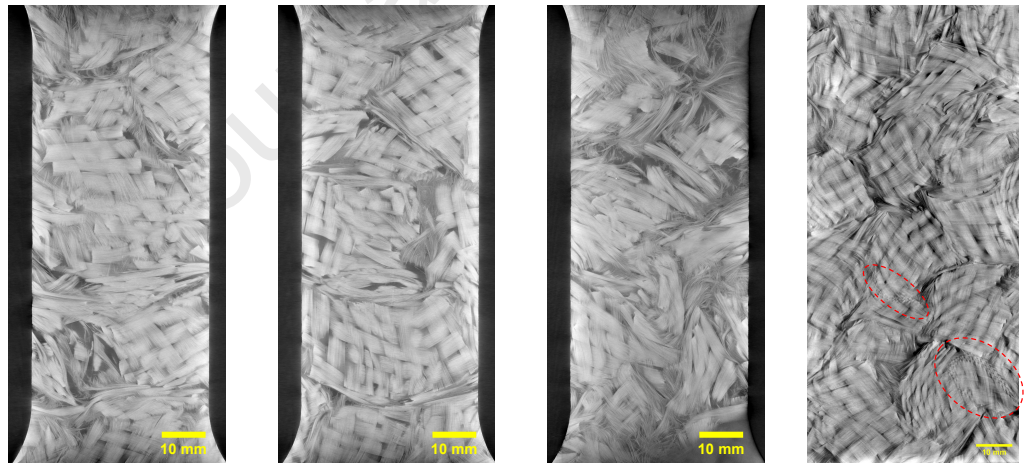

Figure 19: Variability of the composite microstructure observed at different relative out-of-plane coordinates z* with respect to the total thickness (a, b and c). Subfigure (d) demonstrates an extreme microstructure configuration where different architectures of the reinforcement are observed.

The new implementation considers a correction coefficient λ that accounts for the microstructural complexity of the strands, and the degradation that the chips undergo during processing. It is obtained through a calibration process minimizing the error between the predicted and the experimental moduli. It enters only in the first step of homogenization (properties of strands, which are assumed unidirectional fiber composites). Once this step is fulfilled, the overall response of the composite is estimated using the periodic homogenization framework of subsections 4.1.2 and 4.1.3. After the calibration, recovered Young's and shear moduli values after micro-homogenization are reduced by $\lambda = 35\%$. To obtain this value, several computations with different reduction coefficients are performed and the percentage errors for the elastic moduli are calculated. The results are presented in figure 20 and show that the lowest error values are achieved using a 35% reduction. The model's simulations approached the experimental values closely by using this value. The formula used for percentage error calculation is the following:

$$\text{Percentage Error} = \left(\frac{|\text{Numerical Value} - \text{Experimental Value}|}{\text{Experimental Value}} \right) \times 100 \quad (9)$$

The correction coefficient λ can be expressed using the following formula:

$$\lambda = \text{Argmin} \left| \frac{E_{ii}^{num} - E_{ii}^{exp}}{E_{ii}^{exp}} \right|, \quad i = 1, 2 \quad with \quad \lambda \in \mathbb{R}^{+} \qquad (10)$$

After taking into account fiber degradation via the correction coefficient, Young's moduli for the randomly oriented strand RVEs approach experimental values, as shown in figure 21. The rest of the material constants are shown in table 5. Indeed, it can be observed that imposing a strand generation ODF as well as a correction coefficient significantly reduces the discrepancy between numerical and experimental results. By using the imposed ODF for the generation of RVEs, the approximation error for E_1 reduces to 2.8% and to 2.4% for E_2. Overall, it can be said that good agreement was exhibited between experimental and simulation results for the final version of the model. It also noticed that the obtained effective properties are quite stable independent of the choice of the RVE, contrarily to the case of randomly oriented strands (figure 17).

To better understand the effect of strand length on the effective response of the material, several RVEs are generated with varying strand lengths (L = 20 mm, 30 mm, 40 mm) with a constant width of 20 mm and the same fiber

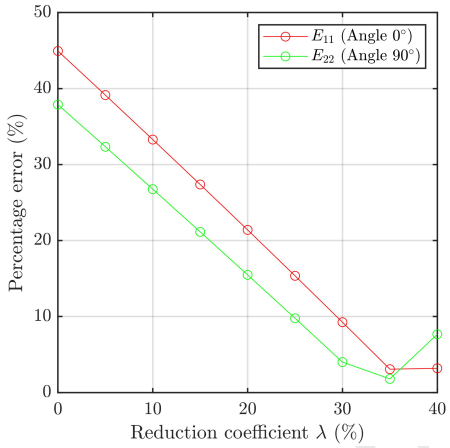

Figure 20: Comparison of percentage error for Young's moduli at various reduction coefficients.

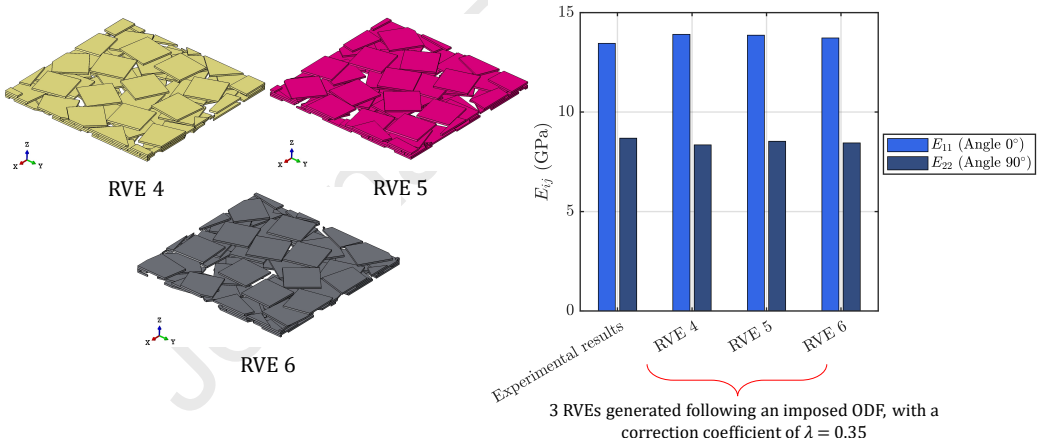

Figure 21: Comparison of experimental and numerical results using a fixed ODF for generating Representative Volume Elements (RVEs), after taking into account fiber degradation. The images of RVEs 4,5 and 6 represent the architecture of the reinforcement.

	E_{11}	E_{22}	E_{33}	ν_{12}	ν_{13}	ν_{23}	G_{12}	G_{13}	G_{23}
RVE 4	13.91	8.45	6.70	0.32	0.22	0.3	4.02	2.42	2.33
RVE 5	13.87	8.53	6.62	0.3	0.23	0.3	4.02	2.41	2.29
RVE 6	13.73	8.46	6.82	0.32	0.22	0.3	4.06	2.48	2.35

Table 5: Material properties of RTPC material obtained using material homogenization; shear and Young's moduli are expressed in GPa.

volume fraction of 47%, as shown in figures 22b, 22c and 22d. The resulting Young's moduli in the 1 and 2 directions for these RVEs are illustrated in figure 22a. The results indicate that an increase in strand length has little to no effect on the effective response of the material. Similar trends have been observed experimentally and discussed previously in section 3.5, for the RTPC-SQR and RTPC-REC materials. Furthermore, similar results were reported in the literature [34].

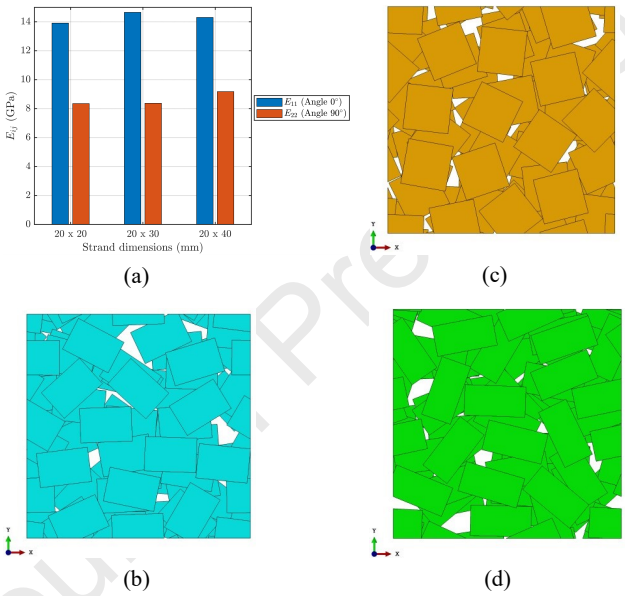

Figure 22: Numerical simulation results obtained for RVEs with different strand length; (b) strand dimensions : 20x20 mm; (c) strand dimensions : 30x20 mm; (d) strand dimensions : 40x20 mm.

5. Conclusions and further work

A detailed investigation of the microstructure of materials mechanically recycled from thermoplastic woven composites was conducted. The investigation was performed using multiple destructive and non-destructive techniques and has shown that the complex material flow phenomena during processing create a particular fiber structure, that can be analyzed on both microscopic and mesoscopic material levels. At the meso scale, the reinforcement is sorted into two observed architectures, in UD strands appearing mostly on the surfaces of the specimens and in woven architecture. The latter is observed

at the center of the plates. Meanwhile, at the microlevel, fibers are packed densely in a unidirectional configuration. Damage mechanisms, crack path and crack surface investigations showed that failure usually appears on the interface of two strands, coupled with damage that is observed at the micro level between fibers.

The collected data from the microstructural investigation of recycled thermoplastic composites has been exploited to develop a multi-scale mechanical model. The latter is able to capture the mechanical response of the material, including the anisotropic behavior observed on the monotonic tensile tests. The microstructural variability and eventually the initial damage induced by the shredding process are accounted for through a correction coefficient. The latter is calibrated by minimizing the scatter between simulation and experimental results.

Future work will focus on investigating and capturing the effect of recycling and processing on the progressive degradation of the composite. In addition, the nonlinear response of the material will be experimentally characterized and implemented into the multi-scale modeling. This could be achieved by incorporating the damage mechanism observations into the model and considering the elastoplastic and viscoplastic natures of the constituent phases at the relevant scale. Several models have been developed by the authors, that take into account strand damage induced by transverse cracking and pseudo-delamination, as well as ductile damage of the thermoplastic matrix and fiber/matrix debonding [50, 51]. Finally, in order to accelerate the development of recycled thermoplastic materials, the proposed multiscale model could be exploited to inform a data-driven approach based on reduction model techniques, such as non-intrusive PGD. This could provide a real-time overall response prediction for recycled thermoplastic composites, for different fiber and matrix materials as well as different geometric parameters.

References

[1] M. Nachtane, M. Tarfaoui, I. Goda, M. Rouway, A review on the technologies, design considerations and numerical models of tidal current turbines, Renewable Energy 157 (2020) 1274–1288.

[2] M. Biron, Thermoplastics and thermoplastic composites, William Andrew, 2018.

[3] M. Nachtane, M. Tarfaoui, M. amine Abichou, A. Vetcher, M. Rouway, A. Aâmir, H. Mouadili, H. Laaouidi, H. Naanani, An overview of the recent advances in composite materials and artificial intelligence for hydrogen storage vessels design, Journal of Composites Science 7 (2023) 119.

[4] E. Asmatulu, J. Twomey, M. Overcash, Recycling of fiber-reinforced composites and direct structural composite recycling concept, Journal of Composite Materials 48 (2014) 593–608.

[5] M. E. Otheguy, A. G. Gibson, E. Findon, R. M. Cripps, A. O. Mendoza, M. T. A. Castro, Recycling of end-of-life thermoplastic composite boats, Plastics, Rubber and Composites 38 (2009) 406–411.

[6] P. Corvaglia, A. Passaro, O. Manni, L. Barone, A. Maffezzoli, Recycling of pp-based sandwich panels with continuous fiber composite skins, Journal of Thermoplastic Composite Materials 19 (2006) 731–745.

[7] M. F. Khurshid, M. Hengstermann, M. M. B. Hasan, A. Abdkader, C. Cherif, Recent developments in the processing of waste carbon fibre for thermoplastic composites–a review, Journal of Composite Materials 54 (2020) 1925–1944.

[8] J. L. Thomason, L. Yang, R. Meier, The properties of glass fibres after conditioning at composite recycling temperatures, Composites Part A: Applied Science and Manufacturing 61 (2014) 201–208.

[9] P. Kiss, W. Stadlbauer, C. Burgstaller, H. Stadler, S. Fehringer, F. Haeuserer, V.-M. Archodoulaki, In-house recycling of carbon- and glass fibre-reinforced thermoplastic composite laminate waste into high-performance sheet materials, Composites Part A: Applied Science and Manufacturing 139 (2020) 106110.

[10] A. E. Krauklis, C. W. Karl, A. I. Gagani, J. K. Jørgensen, Composite material recycling technology—state-of-the-art and sustainable development for the 2020s, Journal of Composites Science 5 (2021) 28.

[11] G. Oliveux, L. O. Dandy, G. A. Leeke, Current status of recycling of fibre reinforced polymers: Review of technologies, reuse and resulting properties, Progress in materials science 72 (2015) 61–99.

[12] M. I. A. Rasheed, Compression molding of chopped woven thermoplastic composite flakes (2016).

[13] R. Chekkour, A. Benaarbia, G. Chatzigeorgiou, F. Meraghni, G. Robert, Effect of thermo-hygro glycol aging on the damage mechanisms of short glass-fiber reinforced polyamide 66, Composites Part A: Applied Science and Manufacturing 165 (2023) 107358.

[14] A. Benaarbia, G. Chatzigeorgiou, B. Kiefer, F. Meraghni, A fully coupled thermo-viscoelastic-viscoplastic-damage framework to study the cyclic variability of the taylor-quinney coefficient for semi-crystalline polymers, International Journal of Mechanical Sciences 163 (2019) 105128.

[15] N. Miqoi, P. Pomarede, F. Meraghni, N. F. Declercq, L. Guillaumat, G. L. Coz, S. Delalande, Detection and evaluation of barely visible impact damage in woven glass fabric reinforced polyamide 6.6/6 composite using ultrasonic imaging, x-ray tomography and optical profilometry, International Journal of Damage Mechanics 30 (2021) 323–348.

[16] P. Marguères, F. Meraghni, Damage induced anisotropy and stiffness reduction evaluation in composite materials using ultrasonic wave transmission, Composites Part A: Applied Science and Manufacturing 45 (2013) 134 – 144.

[17] R. M. Gonçalves, A. Martinho, J. P. Oliveira, Recycling of reinforced glass fibers waste: Current status, Materials 15 (2022) 1596.

[18] G. Colucci, O. Ostrovskaya, A. Frache, B. Martorana, C. Badini, The effect of mechanical recycling on the microstructure and properties of pa66 composites reinforced with carbon fibers, Journal of Applied Polymer Science 132 (29) (2015).

[19] B. Franzen, C. Klason, J. Kubat, T. Kitano, Fibre degradation during processing of short fibre reinforced thermoplastics, Composites 20 (1) (1989) 65–76.

[20] A. D. L. Subasinghe, R. Das, D. Bhattacharyya, Fiber dispersion during compounding/injection molding of pp/kenaf composites: Flammability and mechanical properties, Materials Design 86 (2015) 500–507.

[21] R. J. Tapper, M. L. Longana, I. Hamerton, K. D. Potter, A closed-loop recycling process for discontinuous carbon fibre polyamide 6 composites, Composites Part B: Engineering 179 (2019) 107418.

[22] G. Schinner, J. Brandt, H. Richter, Recycling carbon-fiber-reinforced thermoplastic composites, Journal of Thermoplastic Composite Materials 9 (1996) 239–245.

[23] N. Eguemann, L. Giger, M. Roux, C. Dransfeld, F. Thiebaud, D. Perreux, Compression moulding of complex parts for the aerospace with discontinuous novel and recycled thermoplastic composite materials, 19th international conference on composite materials (2013) 1–11.

[24] D. D. Howell, S. Fukumoto, Compression molding of long chopped fiber thermoplastic composites, 2014, pp. 13–16.

[25] S. B. Visweswaraiah, M. Selezneva, L. Lessard, P. Hubert, Mechanical characterisation and modelling of randomly oriented strand architecture and their hybrids–a general review, Journal of Reinforced Plastics and Composites 37 (2018) 548–580.

[26] L. T. Harper, C. C. Qian, R. Luchoo, N. A. Warrior, 3d geometric modelling of discontinuous fibre composites using a force-directed algorithm, Journal of Composite Materials 51 (2017) 2389–2406.

[27] H. Tang, G. Zhou, Z. Chen, L. Huang, K. Avery, Y. Li, H. Liu, H. Guo, H. Kang, D. Zeng, Fatigue behavior analysis and multi-scale modelling of chopped carbon fiber chip-reinforced composites under tension-tension loading condition, Composite Structures 215 (2019) 85–97.

[28] M. Nachtane, F. Meraghni, G. Chatzigeorgiou, L. Harper, F. Pelascini, Multiscale viscoplastic modeling of recycled glass fiber-reinforced thermoplastic composites: Experimental and numerical investigations, Composites Part B: Engineering 242 (2022) 110087.

[29] Cetim, Recyclage des matériaux polymères et composites thermoplastiques, `https://rb.gy/8qjnrs` (Accès le 18/08/2021).

[30] J. L. Thomason, M. A. Vlug, Influence of fibre length and concentration on the properties of glass fibre-reinforced polypropylene: 1. tensile and flexural modulus, Composites Part A: Applied science and manufacturing 27 (1996) 477–484.

[31] S. Garcea, Y. Wang, P. Withers, X-ray computed tomography of polymer composites, Composites Science and Technology 156 (2018) 305–319.

[32] Y. Chemisky, F. Meraghni, N. Bourgeois, S. Cornell, R. Echchorfi, E. Patoor, Analysis of the deformation paths and thermomechanical parameter identification of a shape memory alloy using digital image correlation over heterogeneous tests, International Journal of Mechanical Sciences 96 (2015) 13–24.

[33] F. Meraghni, H. Nouri, N. Bourgeois, C. Czarnota, P. Lory, Parameters identification of fatigue damage model for short glass fiber reinforced polyamide (pa6-gf30) using digital image correlation, Procedia Engineering 10 (2011) 2110–2116.

[34] Y. Wan, J. Takahashi, Tensile and compressive properties of chopped carbon fiber tapes reinforced thermoplastics with different fiber lengths and molding pressures, Composites Part A: Applied Science and Manufacturing 87 (2016) 271–281.

[35] Y. Pan, L. Iorga, A. A. Pelegri, Analysis of 3d random chopped fiber reinforced composites using fem and random sequential adsorption, Computational Materials Science 43 (2008) 450–461.

[36] P. R. K. Mohan, M. A. Kumar, P. M. Mohite, Representative volume element generation and its size determination for discontinuous composites made from chopped prepregs, Composite Structures 252 (2020) 112633.

[37] B. Widom, Random sequential addition of hard spheres to a volume, The Journal of Chemical Physics 44 (1966) 3888–3894.

[38] J.-C. Michel, H. Moulinec, P. Suquet, Effective properties of composite materials with periodic microstructure: a computational approach, Computer methods in applied mechanics and engineering 172 (1999) 109–143.

[39] M. E. F. Idrissi, F. Praud, V. Champaney, F. Chinesta, F. Meraghni, Multiparametric modeling of composite materials based on non-intrusive pgd informed by multiscale analyses: Application for real-time stiffness prediction of woven composites, Composite Structures 302 (2022) 116228.

[40] G. Chatzigeorgiou, Y. Chemisky, F. Meraghni, Computational micro to macro transitions for shape memory alloy composites using periodic homogenization, Smart Materials and Structures 24 (3) (2015) 035009.

[41] G. Chatzigeorgiou, F. Meraghni, N. Charalambakis, Multiscale Modeling Approaches for Composites, Elsevier, 2022.

[42] E. Tikarrouchine, G. Chatzigeorgiou, F. Praud, B. Piotrowski, Y. Chemisky, F. Meraghni, Three-dimensional fe2 method for the simulation of non-linear, rate-dependent response of composite structures, Composite Structures 193 (2018) 165–179.

[43] E. Tikarrouchine, G. Chatzigeorgiou, Y. Chemisky, F. Meraghni, Fully coupled thermo-viscoplastic analysis of composite structures by means of multi-scale three-dimensional finite element computations, International Journal of Solids and Structures 164 (2019) 120–140.

[44] E. Tikarrouchine, A. Benaarbia, G. Chatzigeorgiou, F. Meraghni, Nonlinear fe2 multiscale simulation of damage, micro and macroscopic strains in polyamide 66-woven composite structures: Analysis and experimental validation, Composite Structures 255 (2021) 112926.

[45] D. Anagnostou, G. Chatzigeorgiou, Y. Chemisky, F. Meraghni, Hierarchical micromechanical modeling of the viscoelastic behavior coupled to damage in smc and smc-hybrid composites, Composites Part B: Engineering 151 (2018) 8–24.

[46] M. Barral, G. Chatzigeorgiou, F. Meraghni, R. Léon, Homogenization using modified mori-tanaka and tfa framework for elastoplastic-

viscoelastic-viscoplastic composites: Theory and numerical validation, International Journal of Plasticity 127 (2020) 102632.

[47] Q. Chen, G. Chatzigeorgiou, F. Meraghni, Extended mean-field homogenization of viscoelastic-viscoplastic polymer composites undergoing hybrid progressive degradation induced by interface debonding and matrix ductile damage, International Journal of Solids and Structures 210 (2021) 1–17.

[48] M. Gupta, K. Wang, Fiber orientation and mechanical properties of short-fiber-reinforced injection-molded composites: Simulated and experimental results, Polymer Composites 14 (5) (1993) 367–382.

[49] M. Tarfaoui, S. Choukri, A. Nême, Effect of fibre orientation on mechanical properties of the laminated polymer composites subjected to out-of-plane high strain rate compressive loadings, Composites Science and Technology 68 (2) (2008) 477–485.

[50] F. Praud, G. Chatzigeorgiou, F. Meraghni, Fully integrated multi-scale modelling of damage and time-dependency in thermoplastic-based woven composites, International Journal of Damage Mechanics 30 (2021) 163–195.

[51] Q. Chen, G. Chatzigeorgiou, G. Robert, F. Meraghni, Viscoelastic-viscoplastic homogenization of short glass-fiber reinforced polyamide composites (pa66/gf) with progressive interphase and matrix damage: New developments and experimental validation, Mechanics of Materials 164 (2022) 104081.

AUTHORSHIP STATEMENT Manuscript title:

Experimental and multi-scale investigation of the mechanical behavior of mechanically recycled glass fiber reinforced thermoplastic composites

Saïf Eddine Sekkal: Writing - Original Draft, Formal Analysis, Investigation, Validation

Fodil Meraghni: Conceptualization, Methodology, Writing - Review & Editing, Project administration

George Chatzigeorgiou: Writing - Review & Editing, Methodology, Conceptualization, investigation

Laurent Peltier: Formal Analysis, Investigation, Validation.

Nelly Durand: Resources, Data curation.

Declaration of interests

☒ The authors declare that they have no known competing financial interests or personal relationships that could have appeared to influence the work reported in this paper.

☐The authors declare the following financial interests/personal relationships which may be considered as potential competing interests: